Frontiers in Bioscience Landmark

Front. Biosci. (Landmark Ed) **2026**; 31(1): 46553
https://doi.org/10.31083/FBL46553

Original Research

Gut Microbiota and Metabolome Dynamics Along Gastric Cancer Progression: An Exploratory Multi-Omics Analysis

Jingfang Yang[1,†], Binbin Wang[1,†], Yanfei Yu[1], Hansheng Zhang[1], Xueyong Zhou[1], Guangwen Wu[1], Yan Liu[2], Xiangyang Shi[1,*]

[1]Gastroenterology Department, The People's Hospital of Chizhou, 247100 Chizhou, Anhui, China
[2]Research and Development Center, Center of Human Microecology Engineering and Technology of Guangdong Province, 510700 Guangzhou, Guangdong, China
*Correspondence: shixiangyang2009@126.com (Xiangyang Shi)
[†]These authors contributed equally.
Academic Editor: Amedeo Amedei
Submitted: 13 September 2025 Revised: 22 December 2025 Accepted: 29 December 2025 Published: 20 January 2026

Abstract

Background: Gastric cancer (GC) remains a major global health burden, particularly in East Asia, with complex etiologies involving *Helicobacter pylori* infection, diet, host genetics, and environmental exposures. GC development follows the Correa sequence (CS), a multistep cascade from gastritis to atrophy, erosion, and carcinoma. Although gut microbiota (GM) dysbiosis and metabolic reprogramming have each been implicated in GC, their integrated dynamics across CS remain incompletely defined. **Methods**: We recruited participants across five groups: normal controls (G1), gastritis (G2), atrophy (G3), erosion (G4), and GC (G5). Fecal and gastric tissue samples were analyzed using 16S rRNA sequencing and untargeted metabolomics under both ion modes. Microbial diversity was assessed by α- and β-diversity indices, linear discriminant analysis effect size (LEfSe), and functional prediction. Metabolic features were profiled by UHPLC-Q Exactive Orbitrap MS, and differential metabolites were identified using *t*-tests and partial least squares discriminant analysis (PLS-DA). Diagnostic potential was evaluated using receiver operating characteristic (ROC) curves. **Results**: Microbial α-diversity decreased significantly with progression, particularly in G3, while compositional shifts included depletion of *Bacteroides* and *Faecalibacterium* alongside enrichment of Actinobacteria, Peptostreptococcaceae, and *Lachnoclostridium*. LEfSe identified *Bifidobacterium* and Oscillospiraceae as potential biomarkers of advanced stages. ROC analyses demonstrated strong discriminatory power, with the class *Actinobacteria* achieving an area under the ROC curve (AUC) of 0.935 in distinguishing controls from GC. Fecal metabolomics revealed reductions in anti-inflammatory short-chain fatty acids (SCFAs) and increases in pro-inflammatory metabolites emerging at G3, while tissue metabolomics showed broader reprogramming in GC involving amino acid, nucleotide, lipid, and energy metabolism. Notably, erosion (G4) exhibited transitional features, whereas atrophy (G3) marked a distinct metabolic "breakpoint". **Conclusions**: By integrating GM and metabolomic data, this study delineates stage-specific microbial and metabolic alterations along the CS. Atrophy represents a pivotal inflection point in the transition from homeostasis to carcinogenesis, while erosion serves as a transitional state. Combined microbiota–metabolite signatures hold promise for non-invasive early detection, disease stratification, and mechanistic insights into metabolic dependencies in GC.

Keywords: stomach neoplasms; gastrointestinal microbiome; metabolomics; sequence analysis, DNA; mass spectrometry

1. Introduction

Gastric cancer (GC) is a major global health challenge, with pronounced geographic heterogeneity in incidence and mortality, and a particularly heavy burden in East Asia [1,2]. Although overall GC incidence and mortality have declined worldwide in recent years, GC remains among the leading causes of cancer morbidity and mortality in certain regions such as China, accounting for nearly half of newly diagnosed cases globally [2]. The etiologies of GC are multifactorial, involving *Helicobacter pylori* (*H. pylori*) infection, dietary exposures, host genetic background, and environmental factors [3,4]. Moreover, GC is highly heterogeneous in its clinicopathological presentation, encompassing distinct histological types and molecular features that jointly shape disease progression, therapeutic response, and patient outcomes [5,6].

GC development follows a multistep pathological process known as the Correa sequence (CS). This classical model describes the gradual transition from normal gastric mucosa through chronic gastritis, atrophic gastritis, intestinal metaplasia, and dysplasia, ultimately culminating in intestinal-type GC [7–9]. *H. pylori* infection is considered a principal driver of this cascade, promoting lesion advancement through persistent inflammation and a series of molecular alterations [10,11]. Recent progress in molecular biology and immunology has deepened our understanding of the CS, revealing stage-specific genomic alterations, epigenetic modifications, immune-microenvironment remodeling, and stem-cell-like properties [12]. These advances validate the traditional pathological framework while uncovering more complex mechanisms and heterogeneous trajectories, thereby providing a theoretical basis for early prevention, precision screening, and targeted therapy.

Multiple studies have demonstrated that the gut microbiota (GM) of patients with GC differs markedly from that of healthy individuals, typically characterized by reduced α-diversity, depletion of beneficial taxa, and enrichment of conditionally pathogenic bacteria [13,14]. Such dysbiosis may promote gastric carcinogenesis through several mechanisms, including induction of chronic inflammation, disruption of the mucosal barrier, production of genotoxins, and modulation of the immune microenvironment [15]. For example, *H. pylori* can disturb the gastric microbiome, further disseminate to the intestine, and trigger systemic immune responses [16]. Mendelian randomization analyses have suggested that certain taxa (e.g., *Clostridium sensu stricto 1* and Rikenellaceae) are associated with reduced GC risk, whereas *Roseburia* and the *Eubacterium brachy* group may confer increased risk. Compositional signatures—such as the ratio of *Streptococcus* to *Bacteroides*—can differentiate GC patients from healthy controls, with diagnostic performance (area under the curve, AUC, 0.81–0.86) that may surpass some traditional tumor markers [17]. Microbiota features also track with tumor stage, age, and molecular markers; for instance, alterations are often more pronounced in early GC than in advanced disease, and microbial composition can differ between younger and older patients [18]. Collectively, these findings support the potential of microbiome profiling as a noninvasive diagnostic tool and prognostic indicator. Recent multi-omics studies have begun to unravel the complex microbial and metabolic ecosystem underlying gastric carcinogenesis. For example, a large-scale multi-omics integration [19] demonstrated that dysbiosis-associated depletion of short-chain fatty acid (SCFA) producers coincides with metabolic signatures of inflammation and oxidative stress in early gastric lesions. Another comprehensive atlas combining metagenomics and metabolomics [20] revealed that specific microbial guilds—particularly Streptococcaceae and Lactobacillaceae—shape amino acid and nucleotide metabolic pathways that are progressively rewired along the Correa cascade. Moreover, metabolome-resolved microbiome profiling [21] identified distinct microbial–metabolite co-modules that differentiate gastritis, intestinal metaplasia, and early gastric cancer with high discriminatory accuracy. A recent integrative study [22] further highlighted that microbial shifts in Actinobacteria and Firmicutes strongly correlate with perturbations in bile acid, lipid, and tryptophan metabolism, emphasizing the value of multi-layered omics for mechanistic insight.

Metabolomics studies leveraging plasma, serum, saliva, and other biofluids have identified numerous GC-associated metabolites. For example, a plasma model combining trimethylamine-N-oxide (TMAO) with rhamnose achieved an AUC of 0.961 for discriminating GC [23], while a serum panel composed of acylcarnitines (e.g., C6DC, C16OH) and arginine yielded an AUC of 0.99778 [24]. Salivary metabolomics identified cytosine and 2-oxoglutaric acid as biomarkers with sensitivities exceeding those of some classical serum markers [25]. Moreover, metabolomics of extracellular-vesicle cargo combined with a nanocapture workflow and machine learning achieved highly accurate classification of early GC (AUC = 1.0) [26]. These observations underscore the promise of metabolomics for noninvasive diagnosis.

Despite these advances, several critical knowledge gaps remain. Most previous studies have focused on either the gut microbiota or metabolomics in isolation, without systematically integrating both approaches to delineate stage-specific alterations during GC progression. In particular, the dynamic interplay between microbial dysbiosis and host metabolic reprogramming across the Correa sequence has not been comprehensively characterized. Furthermore, the diagnostic and prognostic utility of combined microbiota–metabolite signatures for early detection and disease stratification remains largely unexplored. Therefore, in this study we aimed to (i) comprehensively characterize gut microbiota composition and metabolic profiles in fecal and gastric tissue samples across different stages of GC; (ii) integrate microbiome and metabolomic data to elucidate key microbe–metabolite–host interaction networks; and (iii) evaluate the diagnostic potential of combined microbial and metabolic features in distinguishing early GC and precancerous lesions from controls. This integrative approach is expected to provide novel insights into the microbiota–metabolism axis in gastric carcinogenesis and may facilitate the development of non-invasive biomarkers for early detection and precision management.

2. Materials and Methods

2.1 Study Population

A total of 93 participants were recruited at The People's Hospital of Chizhou between [March, 2024] and [July, 2024], including normal controls (G1, n = 18), patients with gastritis (G2, n = 22, gastric atrophy (G3, n = 19), gastric erosion (G4, n = 18), and gastric cancer (G5, n = 16). Baseline demographic and clinical data were collected, including age, sex, hematological and biochemical parameters. Exclusion criteria were: (1) use of antibiotics, probiotics, or proton pump inhibitors within 4 weeks; (2) acute infection or autoimmune disease; (3) other malignancies; (4) severe liver, kidney, or metabolic disorders; and (5) gastrointestinal surgery history. All participants provided written informed consent. This study was conducted in accordance with the Declaration of Helsinki, and the study protocol was approved by the Ethics Committee of The People's Hospital of Chizhou (approved No. 2023-KY-17).

H. pylori infection status was determined by either ^{13}C-urea breath testing or histopathological examination of gastric biopsy samples obtained during endoscopy. Dietary information was collected via standardized questionnaires focusing on salt intake, spicy food consumption, and alcohol use. *H. pylori* positivity and basic dietary indicators were incorporated as covariates in subsequent analy-

ses to control for potential confounding effects on the gut microbiota–metabolome associations.

2.2 Sample Collection

Fresh stool samples were collected in sterile containers, immediately frozen at –80 °C, and used for 16S rRNA sequencing and fecal metabolomics. Gastric tissue samples were obtained during gastroscopy or surgery, rinsed in sterile saline, and stored at –80 °C for metabolomic profiling.

2.3 16S rRNA Gene Sequencing and Analysis

Microbial DNA was extracted from stool samples using the QIAamp DNA Stool Mini Kit (Qiagen, Hilden, Germany). The V3–V4 regions of the 16S rRNA gene were amplified with barcoded primers and Pfu high-fidelity DNA polymerase (TransGen Biotech, Beijing, China). PCR products were purified, quantified using the PicoGreen dsDNA assay (Thermo Fisher Scientific, Waltham, MA, USA), and libraries were prepared with the TruSeq Nano DNA LT Library Prep Kit (Illumina, San Diego, CA, USA). Sequencing was performed on the Illumina NovaSeq 6000 (Illumina Inc., San Diego, CA, USA) platform (2 $\times$ 250 bp). Raw reads were processed with fastp (v0.20.0) for quality control. Amplicon sequence variants (ASVs) were generated using DADA2 in QIIME2 (v2023.9), and taxonomy was assigned using the SILVA v138 database. Alpha diversity indices (Chao1, Shannon, Simpson, Pielou's evenness) and beta diversity distances (Bray–Curtis, Jaccard, weighted and unweighted UniFrac) were calculated. Group differences were assessed using Kruskal–Wallis tests (alpha diversity) and PERMANOVA (beta diversity, R^2 = 0.052, p = 0.031). Differential taxa were identified by linear discriminant analysis effect size (LEfSe) with a threshold of LDA >2 and $p < 0.05$. Functional prediction was performed using Tax4Fun2 (v1.1.5, https://tax4fun.gobics.de/).

2.4 Untargeted Metabolomics

Both fecal and tissue metabolites were extracted using cold methanol precipitation, LC-MS grade methanol (Merck, Darmstadt, Germany). Quality control (QC) samples were prepared by pooling aliquots from all study samples and analyzed regularly during the batch to monitor stability. Peaks with detection rate <50% or coefficient of variation >30% in QC were excluded. Metabolomic profiling was performed using UHPLC-Q Exactive Orbitrap MS (Thermo Fisher Scientific, Waltham, MA, USA) under positive (ESI+) and negative (ESI–) ionization modes. Data were processed with MS-DIAL (v4.90) for peak detection, alignment, and quantification. Metabolites were annotated against public databases (HMDB, MassBank, METLIN) with Metabolomics Standards Initiative (MSI) Level 1–3 confidence. Data preprocessing, normalization, and statistical analyses were performed using R (v4.1.2) and the MetaboAnalyst R package (https://www.metaboanalyst.ca/docs/RTutorial.xhtml, v6.0). Differential metabolites were defined as those with $p < 0.05$, $|\log2FC| \geq 0.58$, and variable importance in projection (VIP) >1 from partial least squares discriminant analysis (PLS-DA). To avoid ambiguity, correlation analyses were performed within specific comparison groups rather than across all samples. Specifically, Spearman correlation analyses were conducted using samples from VS2 (G3 vs G1), whereas the pooled differential metabolites served only as a candidate metabolite set. To control for multiple testing, Benjamini–Hochberg false discovery rate (FDR) correction was applied to all univariate analyses. Metabolites with FDR-adjusted $p < 0.05$ were considered statistically significant, while those meeting nominal $p < 0.05$ but not surviving FDR correction were regarded as exploratory findings and interpreted cautiously. Kyoto Encyclopedia of Genes and Genomes (KEGG) pathway enrichment was conducted using hypergeometric testing with false discovery rate (FDR) correction.

Metabolite annotation followed the Metabolomics Standards Initiative (MSI) guidelines. MSI Level 1 and Level 2 identifications were assigned based on matching retention time and MS/MS spectra to in-house and public databases (HMDB, METLIN, MassBank). MSI Level 3 features were annotated using accurate mass and predicted fragmentation patterns. Only metabolites meeting these criteria were included in downstream integrative analyses.

2.5 Microbiota–Metabolite Correlation Analysis

For integrative cross-omics analysis, differential metabolites from all pairwise group comparisons were first pooled, and duplicate features detected in positive and negative ionization modes were merged to obtain a unified set of differential metabolites. Differential genera were identified using LEfSe at the genus level for each comparison group. Spearman correlation analysis was then performed between all differential genera and the combined differential metabolite set, and the resulting p-values were adjusted using the Benjamini–Hochberg false discovery rate (FDR) procedure. Correlation pairs meeting the significance threshold of $p < 0.01$ (FDR-corrected) were retained, and the corresponding genera and metabolites were visualized using heatmaps to illustrate the microbe–metabolite interaction structure.

2.6 Statistical Analysis

Clinical data were analyzed using SPSS (v26.0, IBM Corp., Armonk, NY, USA) and GraphPad Prism (v9.0, GraphPad Software, San Diego, CA, USA). Continuous variables were expressed as mean $\pm$ SD or median (interquartile range, IQR) and compared using Student's t-test or Mann–Whitney U test. Categorical variables were analyzed using χ^2 or Fisher's exact test. A two-sided $p < 0.05$ was considered statistically significant. For microbiome data, Kruskal–Wallis tests were used for alpha diversity, and PERMANOVA for beta diversity. Differential taxa were identified by LEfSe. For metabolomics, normal-

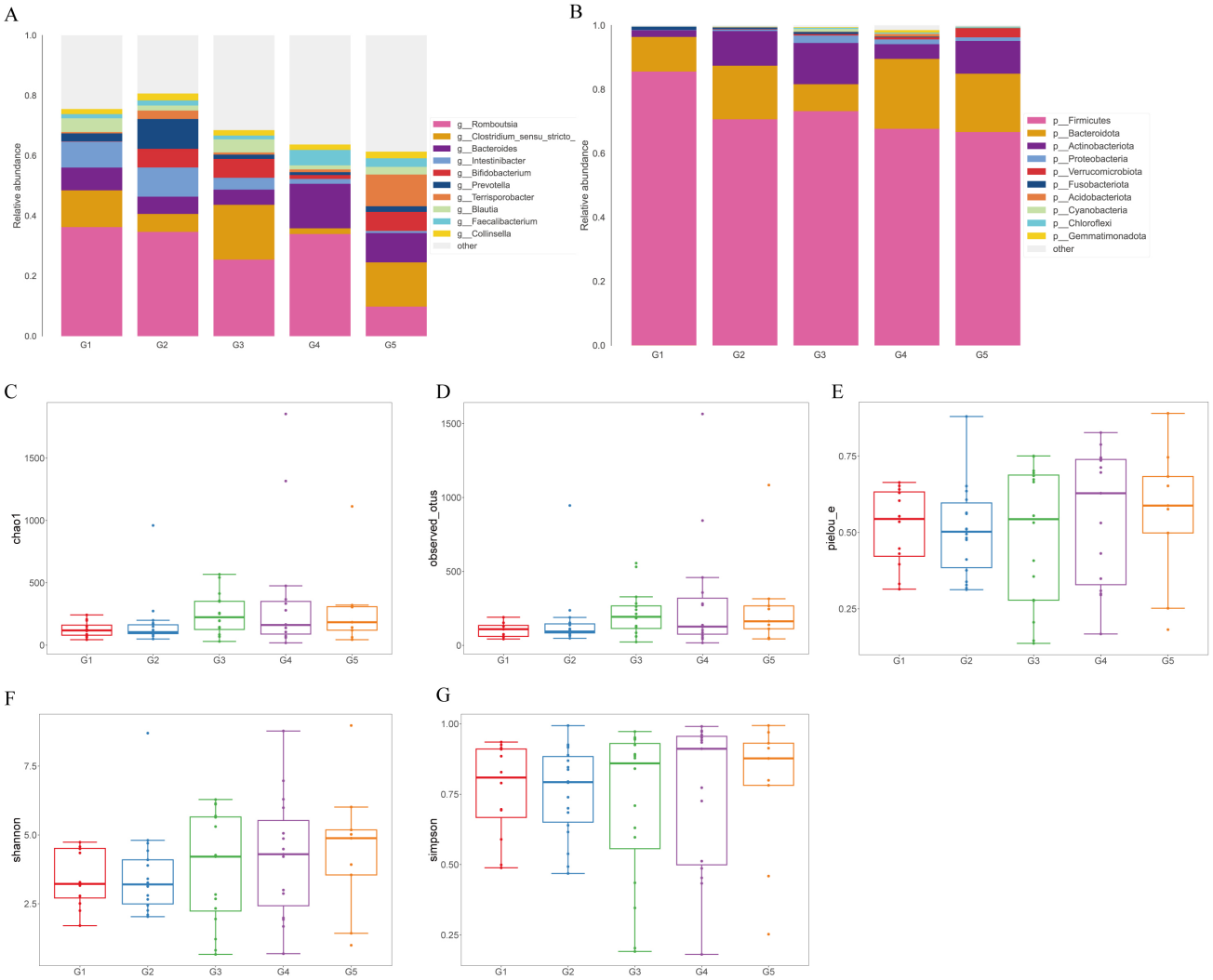

Fig. 1. Gut microbiota composition and alpha diversity across groups. (A) Stacked bar plots showing the relative abundance of the top 10 bacterial phyla across groups (G1–G5). (B) Stacked bar plots showing the relative abundance of the top 10 bacterial genera across groups (G1–G5). (C–G) Alpha diversity indices including Chao1, Observed OTUs, Pielou's evenness (pielou_e), Shannon and Simpson. Error bars represent mean ± SD.

ization was performed by total ion current followed by log transformation. Differential metabolites were identified as described above. Correlations between gut microbial taxa and metabolites were evaluated using Spearman correlation ($|r| > 0.3$, $p < 0.05$).

For clarity, "vs" comparisons in the Results section are defined as follows: vs1 = G1 (normal) vs G2 (gastritis); vs2 = G1 (normal) vs G3 (atrophy); vs3 = G1 (normal) vs G4 (erosion); and vs4 = G1 (normal) vs G5 (gastric cancer). These definitions apply consistently to all α-diversity, β-diversity, LEfSe, and metabolomic analyses.

3. Results

3.1 Baseline Characteristics

Five groups were included: normal controls (G1), gastritis (G2), atrophy (G3), erosion (G4), and GC (G5). The grouping was mainly based on the clinical gastroscopy examination and the HE staining of gastric pathological sections (**Supplementary Figs. 1–5**). The male-to-female ratio did not differ significantly among groups ($p > 0.05$). Age differed significantly ($p = 0.0006$), being lowest in G1 (45 ± 13.53 years) and highest in G5 (67.5 ± 11.97 years), suggesting an association between advancing age and disease progression. Regarding inflammatory markers, C-reactive protein (CRP) did not differ across groups ($p = 0.488$). However, CRP values in G5 showed a markedly skewed distribution (mean ± SD = 4.25 ± 12.46), suggesting the presence of outliers. Therefore, CRP has been reanalyzed and reported as median (interquartile range) to better reflect its non-normal distribution. Among hematologic indices, red blood cell count (RBC) showed significant differences ($p = 0.0104$), with the highest levels in G1 (4.37 ± 0.42 × 10^{12}/L) and the lowest in G5 (3.71 ± 0.57 × 10^{12}/L); white blood cell count (WBC) did not differ significantly ($p = 0.390$). Overall, age increased and RBC declined along the spectrum from normal to GC, whereas

sex ratio, CRP, and WBC remained comparable. Notably, platelet count (PLT) differed significantly among groups ($p = 0.0014$), being lower in the atrophic and erosive stages and increasing again in GC. Although this variation may reflect inflammatory or metabolic responses rather than direct microbiota effects, it was considered as a potential confounding factor in subsequent analyses.

Helicobacter pylori (*H. pylori*) infection status was available for 83 of the 93 participants (89.2%). Infection rates increased progressively with disease stage-11% in G1, 41% in G2, 63% in G3, 67% in G4, and 75% in G5-showing a clear positive association with lesion severity. This variable was incorporated as a covariate in exploratory stratified analyses to minimize potential confounding in the microbiota–metabolome association.

3.2 Gut Microbiota Composition Across Groups

To compare community composition across disease stages, we plotted the top-10 taxa at the phylum (LEVEL2) and genus (LEVEL6) levels for G1–G5 (Fig. 1A,B). At the phylum level, communities were dominated by Firmicutes and Bacteroides across groups. Bacteroides was relatively enriched in G1, whereas Firmicutes gradually became dominant with disease progression and was markedly increased in G5. Actinobacteria and Proteobacteria were also elevated in G5, accompanied by a relative decrease in Bacteroides. At the genus level, G1 was enriched for *Bacteroides* and *Faecalibacterium*, taxa linked to short-chain fatty acid (SCFA) production and anti-inflammatory effects. In G2–G3, several genera within Lachnospiraceae (e.g., *Lachnoclostridium*) increased; in G4, inflammation-associated taxa such as the *Ruminococcus gnavus* group were enriched. In G5, community restructuring was evident with increased Peptostreptococcaceae and *Bifidobacterium*, alongside a marked reduction in *Faecalibacterium*. Altogether, GC progression was characterized by enrichment of Firmicutes, Actinobacteria, and inflammation-related genera, with concurrent depletion of Bacteroides and SCFA producers, indicating a shift toward a pro-inflammatory, pro-carcinogenic microecology.

3.3 Alpha Diversity

We next evaluated alpha diversity using Chao1, Observed OTUs, Shannon, Simpson, and Pielou's evenness. As shown in Fig. 1C–G, both Chao1 and Observed OTUs were significantly reduced in the G1 vs G3 (vs2) comparison, representing the transition from normal mucosa to atrophic gastritis (Chao1: $t = 2.668$, $p = 0.015$; Observed OTUs: $U = 147.0$, $p = 0.019$), indicating a clear decline in richness. By contrast, Shannon and Simpson indices did not differ among groups ($p > 0.4$), suggesting overall diversity and dominance patterns were relatively preserved; Pielou's evenness was also unchanged ($p > 0.5$). Collectively, the vs2 group exhibited reduced richness without major changes in evenness or overall diversity.

3.4 LEfSe Analysis Across Disease Stages

To identify stage-specific microbial biomarkers along GC progression, we performed LEfSe across G1–G5 (Fig. 2). Significant discriminatory features (LDA >2, $p < 0.05$) were detected at multiple taxonomic levels. In G5, the most prominent markers localized to Actinobacteria, including the family Bifidobacteriaceae and genus *Bifidobacterium* (LDA = 3.98, $p = 0.021$). The family Peptostreptococcaceae (Firmicutes) was also enriched (LDA = 3.42, $p = 0.027$), implicating links to tumor-associated metabolism and inflammation. In precancerous stages (G3–G4), enriched taxa included *Lachnoclostridium* (Lachnospiraceae; LDA = 3.11, $p = 0.034$) and the *Ruminococcus gnavus* group (LDA = 2.87, $p = 0.041$), taxa associated with mucosal inflammation and protein metabolism. By contrast, G1 was enriched for *Bacteroides* (Bacteroides; LDA = 3.25, $p = 0.030$) and *Faecalibacterium* (Firmicutes; LDA = 3.54, $p = 0.018$), genera known for SCFA production and anti-inflammatory activity. Overall, LEfSe delineated a shift from SCFA-producing "beneficial" taxa in G1 toward inflammatory and potentially pro-carcinogenic taxa in G3–G5, nominating *Bifidobacterium*, Peptostreptococcaceae, and *Lachnoclostridium* as candidate biomarkers for stage stratification and early screening.

Receiver operating characteristic (ROC) analyses were conducted for each comparison, and the best-performing taxa by AUC were reported (Fig. 3). In VS2 (G1 vs G3), the class Actinobacteria had the highest performance (AUC = 0.81), implicating an association with atrophic lesions. In VS3 (G1 vs G4), the family Muribaculaceae (Bacteroides) achieved an AUC of 0.78. Together, these findings highlight recurring diagnostic value of Actinobacteria across stages, with the strongest performance in VS4 (AUC = 0.94).

3.5 Fecal Untargeted Metabolomics

To characterize metabolic remodeling across stages, we performed multivariate analyses under negative- and positive-ion modes for G1–G5. Partial least squares discriminant analysis (PLS-DA) demonstrated progressive separation of G1 from diseased groups (G2–G5), with increasing distances along the disease continuum (Fig. 4), indicating systemic remodeling of the fecal metabolome. Differential metabolites identified by *t*-test were visualized as volcano plots (Fig. 4C,D). In G2 vs G1, nominally significant differences were observed for several amino-acid derivatives and small molecules in both ion modes; however, After FDR correction, a limited subset of metabolites remained statistically significant, whereas additional nominally altered features ($p < 0.05$, unadjusted) were treated as exploratory and interpreted with caution. In G3 vs G1, *Hexanethioic acid S-propyl ester* remained significant after FDR correction (FDR = 0.0255) in the negative mode, with additional nominal signals among amino-acid derivatives (e.g., N-acetylleucine, N-acetyl-L-tyrosine) and lipid-related molecules (e.g., N-arachidonoyl-leucine), in-

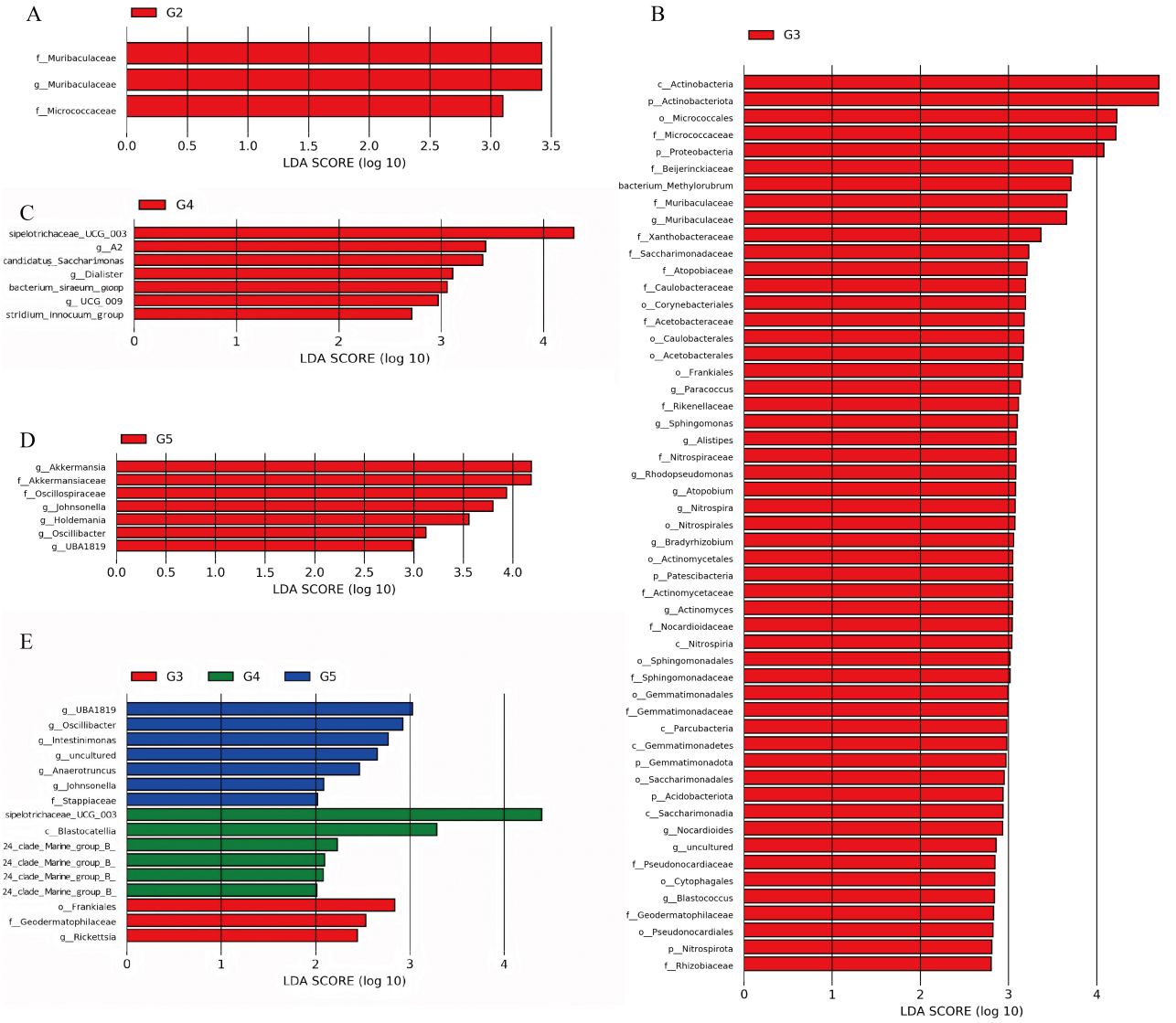

Fig. 2. LEfSe analysis identifies stage-specific microbial biomarkers across disease progression. LDA score bar charts highlight discriminative taxa in group G2 (A), G3 (B), G4 (C), and G5 (D), respectively. (E) Comparative LDA scores of significant biomarkers across groups G3, G4, and G5. Linear Discriminant Analysis Effect Size (LEfSe) was performed with an LDA score threshold >2.

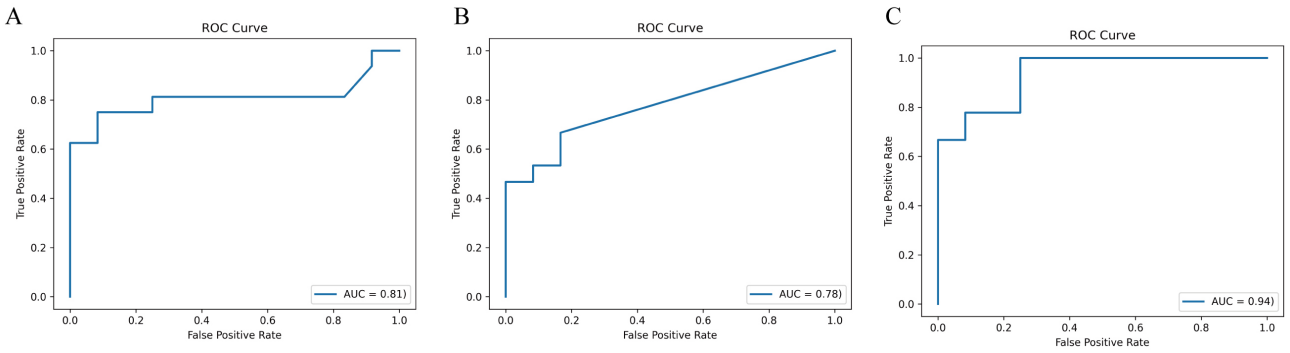

Fig. 3. Diagnostic performance of key taxa. Receiver operating characteristic curves showing the discriminatory power of representative bacterial taxa across group comparisons (VS2–VS4). (A) Actinobacteria. (B) Muribaculaceae. (C) Actinobacteria. The area under the curve (AUC) is indicated for each biomarker.

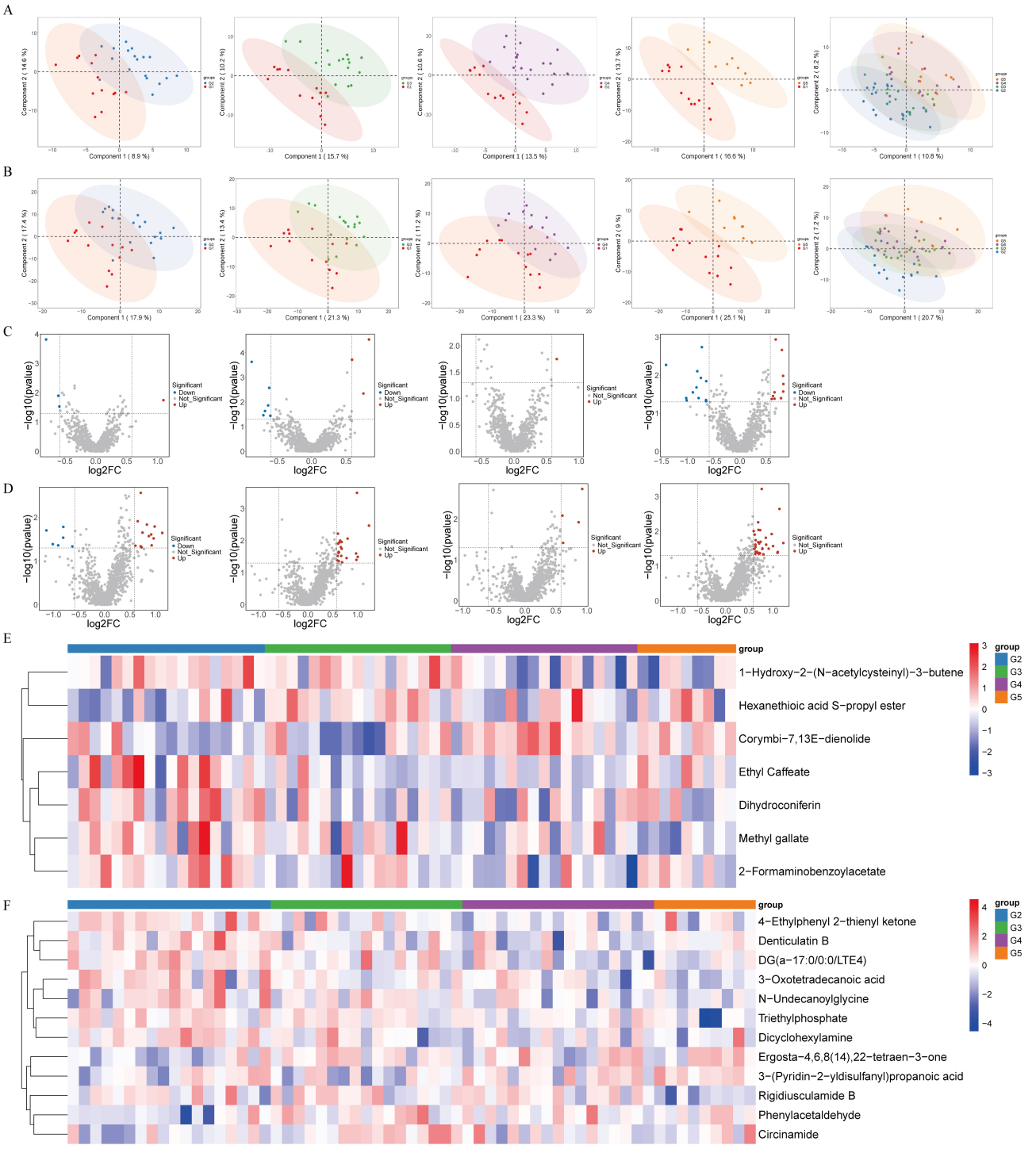

Fig. 4. Fecal untargeted metabolomics analysis. (A,B) Partial least squares discriminant analysis (PLS-DA) score plots of fecal metabolites under negative-ion (A) and positive-ion (B) modes. (C,D) Volcano plots showing differential fecal metabolites in G2 vs G1, G3 vs G1, G4 vs G1, and G5 vs G1 comparisons under negative-ion (C) and positive-ion (D). Red and blue points represent significantly upregulated and downregulated metabolites, respectively ($p < 0.05$, $|\log2FC| \geq 0.58$, VIP >1). (E,F) Heatmaps of significantly altered metabolites across G2–G5 under negative-ion (E) and positive-ion (F) modes. Color gradients in heatmaps indicate relative metabolite abundance (red = upregulated; blue = downregulated). Figures were plotted at 300 dpi with enlarged axis and legend text for readability.

dicating that atrophy represents an early metabolic "breakpoint". In G4 vs G1 and G5 vs G1, more numerous differences were detected, although few passed FDR thresholds; nominal signals were enriched for acetylated amino acids, cofactor-related metabolites, and aromatic derivatives, consistent with a broadening metabolic disturbance rather than a single-metabolite shift. Heatmaps in the positive mode recapitulated these trends: G3 separated most clearly from

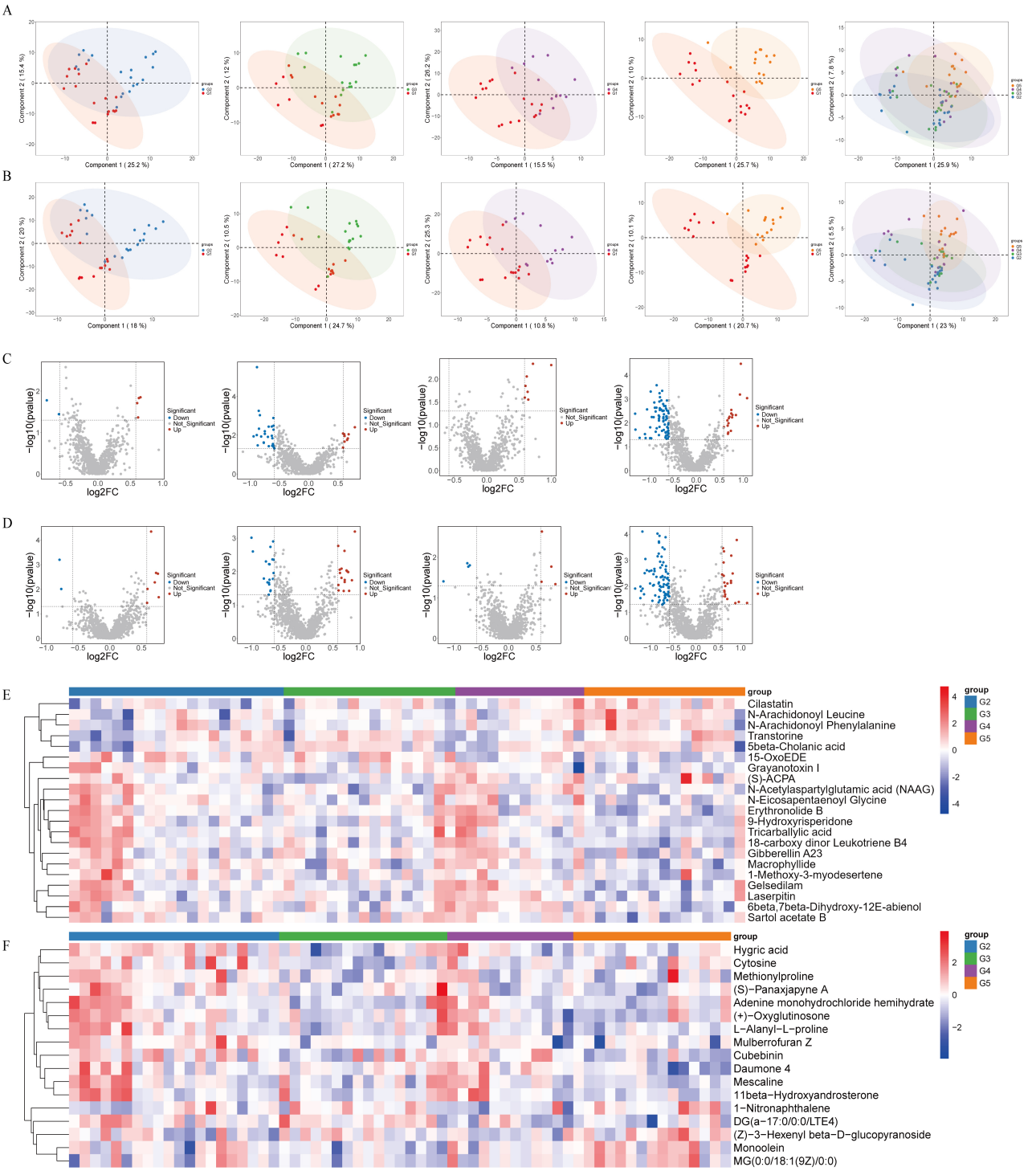

Fig. 5. Tissue untargeted metabolomics analysis. (A,B) Partial least squares discriminant analysis (PLS-DA) score plots of gastric tissue metabolites under negative-ion (A) and positive-ion (B) modes. (C,D) Volcano plots showing differential tissue metabolites in G2 vs G1, G3 vs G1, G4 vs G1, and G5 vs G1 comparisons. Red and blue points represent significantly upregulated and downregulated metabolites, respectively ($p < 0.05$, $|\log2FC| \geq 0.58$, VIP >1). (E,F) Heatmaps of significantly altered metabolites across G2–G5 under negative-ion (E) and positive-ion (F) modes. Color scale bars represent relative intensity ($\log_2$ normalized). All panels have been reformatted for consistent resolution (300 dpi) and legible axis labels.

G1 with widespread perturbations in amino-acid and small-molecule metabolism, while G5 exhibited the most extensive dysregulation involving energy, nucleotide, and lipid reprogramming. Notably, G4 exhibited an intermediate pattern between G3 and G5. This finding suggests that erosion may represent a potential transitional stage in the progression spectrum. Overall, fecal metabolomics indicates prominent abnormalities emerging at the atrophic

stage (G3) and peaking in GC (G5), with G2 and G4 acting as bridges—consistent with microbiome α-diversity and LEfSe findings.

3.6 Tissue Untargeted Metabolomics

To probe local metabolic reprogramming, we profiled gastric tissues across G1–G5 under both ion modes. PLS-DA revealed clear separation among groups (Fig. 5A,B), mirroring fecal results: G1 gradually diverged from G2–G5, with the most pronounced separation for G3 and G5, indicating marked tissue-level remodeling with early abnormalities already evident in precancerous stages. Volcano plots showed a stepwise accumulation of differential metabolites (Fig. 5C,D). G2 vs G1 displayed limited differences (amino-acid and energy-related small molecules), suggesting weak early signals. Although numerous features exhibited nominal significance, only a subset remained significant after FDR adjustment (FDR $<$0.05), primarily involving amino acid and lipid metabolism. These FDR-validated metabolites were subsequently used for KEGG pathway enrichment and correlation analyses. G3 vs G1 showed increased differences centered on amino-acid, lipid, and oxidative-stress pathways, supporting atrophy as a pivotal metabolic inflection. G4 vs G1 exhibited intermediate features—some metabolites approximated G3, others shifted toward G5—consistent with a transitional state. G5 vs G1 yielded the most extensive changes spanning amino-acid, nucleotide, lipid, and energy metabolism, indicative of systemic metabolic reprogramming in tumors. Hierarchical clustering across G2–G5 (Fig. 5E,F) revealed a stepwise trajectory: in the negative mode, G3 and G5 were clearly separated from G1, with G2 and G4 intermediate; in the positive mode, this pattern was more pronounced, with early broad perturbations in G3 and the widest dysregulation in G5, including energy, nucleotide, and membrane-lipid pathways. Taken together, tissue metabolomics reveals prominent abnormalities already at G3 (amino-acid, lipid, and oxidative-stress pathways), which expand into comprehensive reprogramming in G5; G2 and G4 display transitional features. These results suggest that local tissue metabolomes sensitively capture precancerous breakpoints and offer mechanistic clues to microenvironmental remodeling and metabolic dependencies in GC.

3.7 Integrated Microbiota–Metabolite Correlations in the G3 vs G1 Comparison (VS2)

To investigate microbe–metabolite interactions during the transition from non-atrophic to atrophic gastritis, we performed a Spearman correlation analysis between LEfSe-identified differential genera and all differential metabolites in the G3 vs G1 comparison (VS2), followed by FDR correction. Significant associations ($p < 0.01$) are shown in Fig. 6. All correlation analyses were restricted to samples from VS2 (G3 vs G1) to ensure biological interpretability and to avoid confounding effects across disease stages.

A striking interaction pattern emerged in the G3 group. Lipid-related metabolites—including multiple monoacylglycerols (MG18:3, MG18:2, MG20:2), long-chain fatty-acid derivatives (e.g., docosatrienoic acid, arachidonyl ethanolamide, N-arachidonylglycine), and N-acetylated amino-lipid compounds (N-acetylserine, N-acetylvaline)—showed strong positive correlations with several enriched genera such as Alistipes, Akkermansia, Actinomyces, and Bacteroides. These relationships indicate coordinated activation of lipid remodeling pathways at the microbial and metabolic levels.

Amino-acid–related metabolites (including Leu-Ala-Lys, Ile-Thr-Phe, Ala-Leu-Tyr, and threonylproline) also demonstrated significant correlations with the same set of G3-enriched taxa, suggesting enhanced proteolytic or nitrogen-utilization activities. In contrast, taxa such as Muribaculaceae and Nitrosphaera exhibited negative correlations with multiple fatty-acid derivatives, consistent with their reduced abundance in G3 and potential suppression of saccharolytic functions.

Together, these cross-omics correlations highlight coordinated alterations in lipid, fatty-acid, and amino-acid metabolic pathways during the G3 stage and provide hypothesis-generating evidence consistent with G3 as a key metabolic transition point in gastric lesion progression.

4. Discussion

This study systematically delineates dynamic changes in the gut microbiota and metabolites during gastric carcinogenesis, highlighting coordinated and associated changes between specific bacterial taxa and perturbations in related metabolic pathways. We confirm the gradual dysbiosis and metabolic remodeling predicted by the Correa sequence, with microbial and metabolic alterations emerging most prominently at the atrophic stage (G3). In the G1–G3 (vs2) comparison, richness indices (Chao1, Observed OTUs) showed significant reductions ($p < 0.05$), indicating selective loss of low-abundance taxa, while evenness-based indices (Shannon, Simpson, Pielou's) remained stable. This apparent discrepancy between decreased richness and unchanged Shannon/Simpson indices is biologically plausible. Early microbial shifts along the Correa sequence tend to involve the selective loss of low-abundance or conditionally beneficial taxa rather than a redistribution of dominant taxa, resulting in reduced richness but preserved community evenness. Because Shannon and Simpson metrics are more strongly influenced by high-abundance taxa, their stability suggests that the major bacterial groups remain relatively unchanged while rare taxa diminish. Moreover, the continuous, stepwise nature of our cohort—representing adjacent stages of gastric lesion progression rather than binary healthy–cancer contrasts—further explains why subtle richness-focused alterations emerge earlier than changes in overall community uniformity. Beta-diversity analysis by PERMANOVA (Bray–Curtis, $R^2 = 0.052$, $p = 0.031$) further supported compositional divergence from controls beginning at G3.

Fig. 6. Integrated microbiota–metabolite correlation analysis between groups G3 and G1. This figure presents a heatmap that visualizes the significant correlations between differentially abundant microbial genera and differentially abundant metabolites when comparing group G3 (A) to group G1 (B) (comparison set VS2). Heatmap showing significant Spearman correlations ($p < 0.01$, FDR-corrected) between differential genera identified by LEfSe and differential metabolites in the G3 vs G1 group (VS2). *: Represents a correlation with a p-value < 0.05 after False Discovery Rate (FDR) correction, while ** represents $p < 0.01$ and *** represents $p < 0.001$.

Table 1. Baseline clinical and laboratory characteristics.

Variable	G1 (n = 18)	G2 (n = 22)	G3 (n = 19)	G4 (n = 18)	G5 (n = 16)	*p*-value
Male:female	6:12	14:8	10:9	10:8	12:4	/
Age	45 ± 13.53	60 ± 9.65	60 ± 14.86	56.5 ± 9.24	67.5 ± 11.97	0.0006
CRP (mg/L)	1.36 ± 2.17	1.3 ± 14.01	0.9 ± 5.14	0.88 ± 2.39	4.25 ± 12.46	0.4883
RBC ($\times 10^{12}$/L)	4.37 ± 0.42	4.13 ± 0.7	4.13 ± 0.62	4.24 ± 0.69	3.71 ± 0.57	0.0104
WBC ($\times 10^{9}$/L)	5.14 ± 2.42	4.94 ± 1.64	4.55 ± 1.63	4.92 ± 1.69	5.26 ± 1.43	0.3899
NEUT (%)	61.55 ± 10.25	61.55 ± 13.05	60.9 ± 10.85	60.6 ± 9.15	65.35 ± 12.18	0.8217
HGB (g)	128 ± 14.31	125.5 ± 17.65	117 ± 20.98	126.5 ± 22.99	112 ± 25.38	0.0192
HCT (%)	38.5 ± 4.07	38 ± 5.6	37 ± 5.42	38 ± 6.95	33.5 ± 7.62	0.0544
PLT ($\times 10^{9}$/L)	204 ± 62.85	154.5 ± 41.48	146 ± 67.72	179.5 ± 42.42	204.5 ± 57.79	0.0014
ALT (U/L)	22.5 ± 30.46	19 ± 17.74	16 ± 14.76	18.5 ± 14.57	14.5 ± 12.23	0.3897
AST (U/L)	20 ± 15.77	20 ± 22.2	19 ± 11.45	19.5 ± 5.22	17 ± 8.9	0.8311
ALB (g/L)	44.1 ± 4.2	41.55 ± 4.86	39.4 ± 3.97	41.25 ± 4.38	38.8 ± 4.55	0.0057
TBA (µmol/L)	3.05 ± 2.18	4.35 ± 4.75	4 ± 14.69	2.55 ± 2.97	3.15 ± 11.9	0.1913
GGT (U/L)	22.5 ± 15.34	22 ± 67.17	17 ± 32.96	20 ± 13.21	15.5 ± 14.37	0.6758
UA (µmol/L)	276.5 ± 113.25	321 ± 102.13	306 ± 76.88	295.5 ± 91.34	291 ± 73.28	0.6719
BUN (mmol/L)	5.42 ± 1.78	5.03 ± 2.08	4.99 ± 3.2	4.83 ± 2.97	4.58 ± 2.69	0.8493
Cr (µmol/L)	72.25 ± 14.84	83.45 ± 18.65	84.4 ± 134.03	74.65 ± 16.15	82.6 ± 18.69	0.3525
FGB (mmol/L)	4.72 ± 1.03	4.84 ± 1.18	4.76 ± 1.26	4.8 ± 0.61	4.7 ± 0.64	0.988
TT (s)	17.85 ± 1.14	17.7 ± 0.8	18 ± 1	18.2 ± 0.92	17.3 ± 1.02	0.0852
APTT (s)	27 ± 1.74	27.15 ± 2.43	28.4 ± 3.81	26.7 ± 2.56	25.55 ± 3.06	0.4543
PT (s)	10.95 ± 0.77	11.4 ± 0.89	11.5 ± 1.33	11.1 ± 0.56	11.4 ± 0.87	0.1803
Fbg (g/L)	2.56 ± 0.66	2.61 ± 0.92	2.46 ± 0.74	2.51 ± 0.77	3.23 ± 0.76	0.0528
INR	0.94 ± 0.07	0.97 ± 0.39	0.98 ± 0.12	0.94 ± 0.05	0.98 ± 0.08	0.1699
D-D (µg/mL)	0.38 ± 0.59	0.41 ± 0.37	0.31 ± 0.74	0.35 ± 0.19	0.86 ± 1.46	0.0829
USG	1.02 ± 0.01	1.02 ± 0.01	1.02 ± 0.01	1.02 ± 0.01	1.01 ± 0.01	0.0035
BMI (kg/m^2)	22.6 ± 2.4	23.1 ± 2.9	23.4 ± 3.2	22.9 ± 2.7	23.8 ± 3.1	0.428
Current or former smokers, n (%)	2 (11%)	7 (32%)	8 (42%)	9 (50%)	10 (63%)	0.012 *
Current alcohol consumers, n (%)	2 (11%)	5 (23%)	6 (32%)	8 (44%)	9 (56%)	0.018 *
High-salt diet, n (%)	1 (6%)	6 (27%)	8 (42%)	7 (39%)	9 (56%)	0.021 *
[#]*H. pylori* positive, n (%)	2 (11%)	9 (41%)	12 (63%)	12 (63%)	12 (75%)	-

*Significant difference between groups ($p < 0.05$).

[#]*H. pylori* infection was assessed by ^{13}C-urea breath test or histopathology of gastric biopsy during endoscopy. Data available for 83 of 93 participants (89.2%).

In parallel, both fecal and tissue metabolomics revealed the first consistent appearance of amino acid– and lipid-related alterations at this stage, which persisted or amplified through erosion (G4) and GC (G5). These convergent microbial and metabolic signals suggest that atrophy represents an emerging inflection point—rather than an abrupt breakpoint—marking the onset of sustained ecological and metabolic remodeling along gastric carcinogenesis. Erosion (G4) appears to act as a transitional phenotype, bridging atrophic dysbiosis and tumor-associated reprogramming. We further demonstrate that combined microbiota–metabolite signatures have potential value for early diagnosis and disease stratification. Our findings are consistent with and extend recent multi-omics studies that have characterized the microbial–metabolic landscape of gastric cancer. A multi-center analysis [19] reported early depletion of SCFA-producing bacteria accompanied by inflammatory metabolic signatures, aligning with our observation that richness declines at the atrophic stage while SCFA-related metabolites decrease. Another integrative framework [20] highlighted microbial networks involving Streptococcaceae and Lactobacillaceae as key drivers of amino acid reprogramming; similarly, we observed enrichment of Streptococcus-related taxa in erosive and cancer stages together with amino acid and lipid pathway disruptions. Furthermore, stage-specific metabolite–microbe modules identified in a multi-layered cohort [21] mirror our finding that atrophy represents a pivotal metabolic inflection point, with erosion functioning as a transitional phenotype. A recent metagenomic–metabolomic coupling study [22] reported strong associations between Actinobacteria expansion and dysregulated bile acid and tryptophan metabolism, which is consistent with our ROC-identified role of Actinobacteria and the observed perturbations in these metabolic pathways.

We acknowledge that several clinical covariates may influence microbiome and metabolome variation, and have therefore expanded our analysis to better account for potential confounding. Platelet counts, systemic inflammatory markers, BMI, *H. pylori* infection status, smoking and alco-

hol consumption, and dietary salt intake were incorporated into Table 1 and examined for differences across groups. Although none of these variables fully explained the observed multi-omic patterns, their potential contributions—particularly inflammation-related indices—should be considered when interpreting the results. Given the modest sample size and cross-sectional design, residual confounding cannot be excluded, and future longitudinal studies with stratified or multivariable modeling will be needed to more precisely quantify the effects of these clinical factors on microbiome–metabolome interactions.

Beyond biological interpretation, the combined microbiota–metabolite signatures identified in this study have meaningful clinical translational potential. Such integrative markers could be particularly useful for screening individuals at high risk for gastric cancer—such as those with chronic gastritis, atrophic gastritis, or long-term *H. pylori* infection—by enabling non-invasive detection of early mucosal alterations before endoscopically visible lesions emerge. In addition, these signatures may serve as dynamic indicators for monitoring the evolution of precancerous lesions, providing a complementary tool to endoscopy for risk stratification and longitudinal surveillance. From a feasibility perspective, fecal sample collection is simple, low-cost, and well accepted by patients, and the workflow for 16S rRNA sequencing and standardized metabolomics is becoming increasingly accessible in clinical laboratories. As sequencing and mass spectrometry costs continue to decline, these combined markers could be incorporated into routine population-level screening programs or follow-up algorithms for high-risk cohorts. Thus, the translational potential of microbiota–metabolite profiling extends beyond mechanistic insights and may inform real-world strategies for early detection, disease monitoring, and precision prevention.

Microbiome analyses revealed a decline in α-diversity and progressive restructuring of community composition. Controls were enriched for SCFA-producing genera (*Bacteroides*, *Faecalibacterium*), whereas disease stages featured increased Firmicutes, Actinobacteria, and inflammation-related taxa. These patterns align with prior work suggesting that dysbiosis can disrupt the mucosal barrier, sustain chronic inflammation, and accumulate genotoxic metabolites, thereby promoting gastric carcinogenesis [27,28]. Interestingly, the enrichment of Bifidobacterium observed in advanced stages (G5) warrants a nuanced interpretation. Although Bifidobacterium is traditionally regarded as a probiotic genus with anti-inflammatory and immunostimulatory properties, recent studies highlight its strain- and context-dependent roles in tumor biology. Certain strains can enhance antitumor immunity and improve immune checkpoint inhibitor efficacy through STING and interferon signaling pathways, whereas others have been identified within tumor tissues as colonizers of hypoxic or necrotic niches, likely reflecting ecological adaptation rather than causation. Reports in gastric cancer cohorts are also mixed—some showing enrichment, others depletion—depending on sampling site (stool vs. mucosa), tumor stage, *H. pylori* infection, and medication exposure. Therefore, the observed increase in Bifidobacterium in G5 should be interpreted as an ecological signal rather than a uniformly deleterious event. Notably, the atrophic stage (G3) concentrated the most salient microbial shifts, supporting its role as a critical node where "microbiota–host interactions" transition from homeostasis to carcinogenesis.

At the metabolomic level, both fecal and tissue profiles exhibited stage-wise perturbations. Fecal data suggested reductions in anti-inflammatory SCFAs and increases in pro-inflammatory or pro-carcinogenic metabolites (e.g., kynurenine pathway intermediates, secondary bile acids) emerging already at G3. Tissue profiles revealed broader reprogramming in GC, including energy, nucleotide, and lipid metabolism, consistent with proliferative demands and immune evasion. Importantly, all metabolomic analyses were corrected for multiple testing using the Benjamini–Hochberg FDR procedure, and biological interpretations were based primarily on metabolites passing the FDR <0.05 threshold. Nominally significant findings were described only as exploratory observations pending further validation. In line with earlier studies in serum, saliva, and extracellular vesicles [29,30], our findings reinforce the value of multi-omics integration for pinpointing metabolic inflection points and candidate biomarkers.

Correlative analyses linked depletion of SCFA producers to reduced mucosal immunity and altered signaling patterns that were associated with lesion advancement. Within the Correa framework, *H. pylori*-driven chronic inflammation likely perturbs gastric and intestinal communities, with metabolite shifts subsequently modulating local immunity and signaling to accelerate lesion advancement [31,32].

Importantly, ROC analyses indicated that specific taxa (e.g., class Actinobacteria, family Oscillospiraceae) and metabolite combinations (e.g., butyrate + kynurenine + secondary bile acids) achieved good discrimination among controls, precancerous lesions, and GC (AUCs >0.75). The class Actinobacteria reached an AUC of 0.935 for control versus GC, underscoring its potential as a non-invasive biomarker. Compared with single-modality approaches, combined microbiota–metabolite signatures may improve early screening accuracy and stratification robustness.

The integrative correlation analysis of the G3 vs G1 comparison revealed biologically coherent microbe–metabolite modules that reflect functional remodeling during the early atrophic stage. The strong positive associations between Alistipes, Akkermansia, Actinomyces, and Bacteroides with lipid-related metabolites—including monoacylglycerols and arachidonic-acid derivatives—suggest enhanced lipid turnover, altered membrane remodeling, and possible activation of inflammation-linked lipid pathways in G3. The parallel enrichment of

amino-acid metabolites and their correlations with G3-enriched taxa further imply increased proteolytic activity and nitrogen metabolism. Conversely, the negative associations observed for Muribaculaceae and Nitrosphaera with several lipid metabolites are consistent with the decline of saccharolytic functionalities reported in early atrophic gastritis. Although the PERMANOVA effect sizes were modest, which is common in microbiome studies, the coordinated shifts observed at G3 suggest that this stage may represent a potential transitional or acceleration point rather than a discrete inflection boundary.

This study has limitations. First, the sample size is modest; some findings did not remain significant after multiple-testing correction and require validation in larger cohorts. Second, the cross-sectional design precludes causal inference; longitudinal studies and mechanistic models are needed. In addition, although we incorporated available data on *H. pylori* infection and basic dietary habits into exploratory analyses, residual confounding cannot be fully excluded. Future large-scale longitudinal studies should incorporate comprehensive dietary assessment and *H. pylori* stratification to refine the microbiota–metabolome interaction models. Third, metabolite annotation is inherently limited; some features lack definitive pathway mapping. Moreover, because the present study is exploratory and cross-sectional with a modest sample size, advanced causal inference analyses such as co-abundance network modeling and mediation effect testing were not performed, and will be addressed in future longitudinal studies with expanded cohorts. Additionally, the functional roles of key microbial biomarkers identified by LEfSe (such as Bifidobacterium and Streptococcaceae) were not experimentally validated through *in vitro* assays or animal models, and future studies will incorporate bacterial culture supernatant experiments and gnotobiotic or microbiota-transplant models to strengthen causal inference. To overcome these limitations, future work will employ a longitudinal cohort design with repeated sampling across the Correa sequence to capture temporal microbial and metabolic dynamics. Integration of metagenomics, metatranscriptomics, and targeted metabolomics will enable higher-resolution functional mapping of microbial metabolism and host signaling.

In parallel, gnotobiotic mouse and antibiotic-treated models will be used to verify causality between specific taxa (e.g., Actinobacteria, SCFA-producing bacteria) and gastric mucosal inflammation or metabolic reprogramming through immune and signaling pathways such as NF-κB, AMPK/mTOR, and cytokine networks. Finally, expansion of cohort size and implementation of machine-learning-based integrative frameworks will improve the robustness and predictive value of microbiota–metabolite signatures for early GC detection and risk stratification. Furthermore, while our findings reveal clear associations between gut microbial shifts, SCFA depletion, and metabolic remodeling along the Correa sequence, the causal mechanisms remain to be elucidated. In particular, whether decreased SCFAs exacerbate mucosal inflammation via NF-κB or cytokine signaling, and how Actinobacteria enrichment may shape metabolic dependencies through AMPK/mTOR or immune-modulatory pathways, warrants further mechanistic validation. Future studies integrating metatranscriptomics, targeted metabolomics, and immune assays in cellular and animal models are planned to elucidate these regulatory networks. Future work should combine targeted validation, deeper multi-omics (transcriptomics/proteomics), and functional assays to elucidate causal "microbiota–metabolism–host" mechanisms in GC.

5. Conclusion

In summary, by integrating fecal and tissue untargeted metabolomics with 16S profiling, we chart a stage-resolved "microbiota–metabolite–host" interaction landscape across GC progression. Our results suggest that atrophy (G3) may represent a potential inflection stage, whereas erosion (G4) exhibits transitional features. Combined microbial and metabolic features show promise for early detection and stratified management, while offering mechanistic insights into metabolic dependencies that could inform precision prevention and therapy.

Availability of Data and Materials

The datasets used and analyzed during the current study are available from the corresponding author on reasonable request.

Author Contributions

JY and XS conceived and designed the research. BW and YL performed the experiments. YY, HZ, XZ and GW analyzed the results and data. JY and BW wrote, YL and XS revised the manuscript. All authors contributed to editorial changes in the manuscript. All authors read and approved the final manuscript. All authors have participated sufficiently in the work and agreed to be accountable for all aspects of the work.

Ethics Approval and Consent to Participate

This study was approved by the ethics committee of The People's Hospital of Chizhou City (approved No. 2023-KY-17). We certify that the study was performed in accordance with the 1964 declaration of HELSINKI and later amendments. Written informed consent to participate in this study was provided by the patients or their families/legal guardian.

Acknowledgment

We thank Zhao Zhang and Yan Ma (Center of Human Microecology Engineering and Technology of Guangdong Province, Guangdong Longsee Biomedical Corporation, Guangzhou, China) for statistical consultation and technical support provided by the Longseek high-throughput zebrafish screening platform for drug and probiotic evalua-

tion. Also we acknowledge Dr. Shihao Huang from Hainan University for language polishing.

Funding

This study was funded by 2023 Chizhou City major science and technology special project.

Conflict of Interest

The authors declare no conflict of interest.

Declaration of AI and AI-Assisted Technologies in the Writing Process

During the preparation of this work the authors used Deepseek-R1 in order to check spell and grammar. After using this tool, the authors reviewed and edited the content as needed and takes full responsibility for the content of the publication.

Supplementary Material

Supplementary material associated with this article can be found, in the online version, at https://doi.org/10.31083/FBL46553.

References

[1] Mithany RH, Shahid MH, Manasseh M, Saeed MT, Aslam S, Mohamed MS, *et al*. Gastric Cancer: A Comprehensive Literature Review. Cureus. 2024; 16: e55902. https://doi.org/10.7759/cureus.55902.

[2] Yang WJ, Zhao HP, Yu Y, Wang JH, Guo L, Liu JY, *et al*. Updates on global epidemiology, risk and prognostic factors of gastric cancer. World Journal of Gastroenterology. 2023; 29: 2452–2468. https://doi.org/10.3748/wjg.v29.i16.2452.

[3] Gao S, Wei G, Ma Q, Wang X, Wang S, Niu Y. Causal relationship between anti-inflammatory drugs and cancer: a pan-cancer study with Mendelian randomization. Frontiers in Genetics. 2024; 15: 1392745. https://doi.org/10.3389/fgene.2024.1392745.

[4] Morais S, Costa A, Albuquerque G, Araújo N, Tsugane S, Hidaka A, *et al*. "True" Helicobacter pylori infection and non-cardia gastric cancer: A pooled analysis within the Stomach Cancer Pooling (StoP) Project. Helicobacter. 2022; 27: e12883. https://doi.org/10.1111/hel.12883.

[5] Ma J, Meng Y, Zhou X, Guo L, Fu W. The Prognostic Significance and Gene Expression Characteristics of Gastric Signet-Ring Cell Carcinoma: A Study Based on the SEER and TCGA Databases. Frontiers in Surgery. 2022; 9: 819018. https://doi.org/10.3389/fsurg.2022.819018.

[6] Xing Y, Hosaka H, Moki F, Tomaru S, Itoi Y, Sato K, *et al*. Gender Differences in Patients with Gastric Adenocarcinoma. Journal of Clinical Medicine. 2024; 13: 2524. https://doi.org/10.3390/jcm13092524.

[7] Sugano K, Moss SF, Kuipers EJ. Gastric Intestinal Metaplasia: Real Culprit or Innocent Bystander as a Precancerous Condition for Gastric Cancer? Gastroenterology. 2023; 165: 1352–1366.e1. https://doi.org/10.1053/j.gastro.2023.08.028.

[8] Burke E, Harkins P, Arumugasamy M. Incidence of Gastric Adenocarcinoma in Those With Gastric Atrophy: A Systematic Review. Cureus. 2024; 16: e71768. https://doi.org/10.7759/cureus.71768.

[9] Chivu RF, Melesteu C, Bobirca A, Dumitrescu DA, Melesteu I, Mustatea P, *et al*. Advances in Gastric Carcinogenesis Related to Helicobacter Pylori. Chirurgia (Bucharest, Romania: 1990). 2025; 120: 322–344. https://doi.org/10.21614/chirurgia.3147.

[10] He J, Hu W, Ouyang Q, Zhang S, He L, Chen W, *et al*. Helicobacter pylori infection induces stem cell-like properties in Correa cascade of gastric cancer. Cancer Letters. 2022; 542: 215764. https://doi.org/10.1016/j.canlet.2022.215764.

[11] Fang Z, Zhang W, Wang H, Zhang C, Li J, Chen W, *et al*. Helicobacter pylori promotes gastric cancer progression by activating the TGF-β/Smad2/EMT pathway through HKDC1. Cellular and Molecular Life Sciences: CMLS. 2024; 81: 453. https://doi.org/10.1007/s00018-024-05491-x.

[12] Li F, Wang Y, Ping X, Yin JC, Wang F, Zhang X, *et al*. Molecular evolution of intestinal-type early gastric cancer according to Correa cascade. Journal of Biomedical Research. 2024; 39: 270–285. https://doi.org/10.7555/JBR.38.20240118.

[13] Marashi A, Hasany S, Moghimi S, Kiani R, Mehran Asl S, Dareghlou YA, *et al*. Targeting gut-microbiota for gastric cancer treatment: a systematic review. Frontiers in Medicine. 2024; 11: 1412709. https://doi.org/10.3389/fmed.2024.1412709.

[14] He Y, Gao S, Jiang L, Yang J. Changes in gut microbiota after gastric cancer surgery: a prospective longitudinal study. Frontiers in Oncology. 2024; 14: 1533816. https://doi.org/10.3389/fonc.2024.1533816.

[15] Chen Z, Jin D, Hu J, Guan D, Bai Q, Gou Y. Microbiota and gastric cancer: from molecular mechanisms to therapeutic strategies. Frontiers in Cellular and Infection Microbiology. 2025; 15: 1563061. https://doi.org/10.3389/fcimb.2025.1563061.

[16] Albush A, Yassine F, Abbas H, Hanna A, Saba E, Bilen M. The impact of *Helicobacter pylori* infection and eradication therapies on gut microbiota: a systematic review of microbial dysbiosis and its implications in gastric carcinogenesis. Frontiers in Cellular and Infection Microbiology. 2025; 15: 1592977. https://doi.org/10.3389/fcimb.2025.1592977.

[17] Xie N, Wang Z, Shu Q, Liang X, Wang J, Wu K, *et al*. Association between Gut Microbiota and Digestive System Cancers: A Bidirectional Two-Sample Mendelian Randomization Study. Nutrients. 2023; 15: 2937. https://doi.org/10.3390/nu15132937.

[18] Chen C, Du Y, Liu Y, Shi Y, Niu Y, Jin G, *et al*. Characteristics of gastric cancer gut microbiome according to tumor stage and age segmentation. Applied Microbiology and Biotechnology. 2022; 106: 6671–6687. https://doi.org/10.1007/s00253-022-12156-x.

[19] Xie J, Xu J, Tian Z, Liang J, Tang H. Extended Insights Into Advancing Multi-Omics and Prognostic Methods for Cancer Prognosis Forecasting. Frontiers in Bioscience (Landmark Edition). 2025; 30: 44091. https://doi.org/10.31083/FBL44091.

[20] Hosseinkhani F, Chevalier C, Marizzoni M, Park R, Bos S, Dunjko AK, *et al*. Plasma and feces multiomics unveil cognition-associated perturbations of chronic inflammatory pathways of the gut-microbiota-brain axis. Alzheimer's & Dementia: the Journal of the Alzheimer's Association. 2025; 21: e70844. https://doi.org/10.1002/alz.70844.

[21] Xie J, Liu M, Deng X, Tang Y, Zheng S, Ou X, *et al*. Gut microbiota reshapes cancer immunotherapy efficacy: Mechanisms and therapeutic strategies. IMeta. 2024; 3: e156. https://doi.org/10.1002/imt2.156.

[22] Liao X, Long J, Wang X, Han K, Tang Z, Chen J, *et al*. Multi-omics reveals cross-tissue regulatory mechanisms of autism risk loci via gut microbiota-immunity-brain axis. AMB Express. 2025; 15: 161. https://doi.org/10.1186/s13568-025-01969-4.

[23] Li D, Lu Y, Zhao F, Yan L, Yang X, Wei L, *et al*. Targeted metabolomic profiles of serum amino acids and acylcarnitines related to gastric cancer. PeerJ. 2022; 10: e14115. https://doi.org/10.7717/peerj.14115.

[24] Li B, Shu X, Jiang H, Shi C, Qi L, Zhu L, *et al*. Plasma metabolome identifies potential biomarkers of gastric precancerous lesions and gastric cancer risk. Metabolomics: Official Journal of the Metabolomic Society. 2023; 19: 73. https://doi.org/10.1007/s11306-023-02037-3.

[25] Nakane K, Yagi K, Yajima S, Nomura S, Sugimoto M, Seto

Y. Salivary metabolomic biomarkers for esophageal and gastric cancers by liquid chromatography-mass spectrometry. Cancer Science. 2024; 115: 3089–3098. https://doi.org/10.1111/cas.16256.

[26] Bu F, Shen X, Zhan H, Wang D, Min L, Song Y, *et al*. Efficient Metabolomics Profiling from Plasma Extracellular Vesicles Enables Accurate Diagnosis of Early Gastric Cancer. Journal of the American Chemical Society. 2025; 147: 8672–8686. https://doi.org/10.1021/jacs.4c18110.

[27] Wang Y, Han W, Wang N, Han M, Ban M, Dai J, *et al*. The role of microbiota in the development and treatment of gastric cancer. Frontiers in Oncology. 2023; 13: 1224669. https://doi.org/10.3389/fonc.2023.1224669.

[28] Sharma P, Phatak SM, Warikoo P, Mathur A, Mahant S, Das K, *et al*. Crosstalk between *Helicobacter pylori* and gastrointestinal microbiota in various gastroduodenal diseases-A systematic review. 3 Biotech. 2023; 13: 303. https://doi.org/10.1007/s13205-023-03734-5.

[29] Zhu J. New Metabolomic Insights Into Cancer. Cancer Journal (Sudbury, Mass.). 2024; 30: 301–306. https://doi.org/10.1097/PPO.0000000000000740.

[30] Liu C, Liu W, Huang J, Wu Z, Li W, Chen B, *et al*. Metabolic Reprogramming Shapes the Progression and Therapeutic Landscape of Ovarian Cancer. Cancer Management and Research. 2025; 17: 1707–1722. https://doi.org/10.2147/CMAR.S538281.

[31] Idowu S, Polglaze K, Van TTH, Moore RJ, Ramsland PA, Bertrand PP, *et al*. Gastric Inflammation Impacts Serotonin Secretion in a Mouse Model of *Helicobacter pylori* Vaccination. International Journal of Molecular Sciences. 2025; 26: 7735. https://doi.org/10.3390/ijms26167735.

[32] Wu D, Cao M, Peng J, Li N, Yi S, Song L, *et al*. The effect of trimethylamine N-oxide on Helicobacter pylori-induced changes of immunoinflammatory genes expression in gastric epithelial cells. International Immunopharmacology. 2017; 43: 172–178. https://doi.org/10.1016/j.intimp.2016.11.032.